Ab initio volume-dependent elastic and lattice dynamical properties of chalcopyrite $CuAlSe_2$

2006 J. Phys.: Condens. Matter 18 1413

(http://iopscience.iop.org/0953-8984/18/4/025)

INSTITUTE OF PHYSICS PUBLISHING JOURNAL OF PHYSICS: CONDENSED MATTER

J. Phys.: Condens. Matter **18** (2006) 1413–1425 doi:10.1088/0953-8984/18/4/025

Ab initio volume-dependent elastic and lattice dynamical properties of chalcopyrite $CuAlSe_2$

Tanju Gürel and Resul Eryiğit

Department of Physics, Abant Izzet Baysal University, Bolu-14280, Turkey

E-mail: resul@ibu.edu.tr

Received 26 September 2005, in final form 8 November 2005
Published 13 January 2006
Online at stacks.iop.org/JPhysCM/18/1413

Abstract

We have performed an *ab initio* study of the volume dependence of elastic and lattice dynamical properties of chalcopyrite semiconductor $CuAlSe_2$. The calculations have been carried out within the local density functional approximation using norm-conserving pseudopotentials and a plane-wave basis. Born effective charge tensors, dielectric permittivity tensors, the phonon frequencies at the Brillouin zone centre and their Grüneisen parameters are calculated using density functional perturbation theory. We compare the Grüneisen parameters of the calculated quantities with those of zinc-blende type materials and find similar trends. Calculated elastic stiffness constants show pseudocubic behaviour.

1. Introduction

The ternary I–III–VI_2 chalcopyrites form a large group of semiconductors with diverse structural, electrical and optical properties [1, 2] and here attracted important attention for a long time because of their large potential in photovoltaic and nonlinear optical applications. Among these compounds, $CuAlSe_2$, with a bandgap of 2.67 eV [3], is promising as an emitting layer of blue light photoluminescent devices [4] as well as a window in heterostructure photovoltaic devices [5].

Experimental determinations of phonon frequencies, elastic stiffness constants, compressibilities and bulk moduli for a number of chalcopyrite compounds have been reported in the literature but the results are often contradictory [6, 7]. The lattice dynamical properties of $CuAlSe_2$ have been studied experimentally by Raman [8–12] and infrared [12–14] spectroscopic methods. The study of characteristic phonon frequencies is one of the most important methods for the characterization of strained materials [15]. The pressure dependence of lattice dynamical properties, such as effective charges, phonon frequencies and low frequency dielectric constants, provides crucial information about the structure of the material. The pressure dependent phonon frequencies of these materials have been investigated to delineate the symmetry assignments of the zone centre modes as well as to give an

understanding of the structural phase transitions at elevated pressures. Among these studies, Gonzalez *et al* [16] have used ZnS as an analogue of $CuGaS_2$ and reported pressure-dependent zone centre phonons up to a pressure of 18.4 GPa. The pressure dependences of structural properties of $CuAlS_2$ and $CuAlSe_2$ were studied by an energy dispersive x-ray diffraction technique by Roa *et al* [17], and $CuAlSe_2$ was found to undergo a transition to a probable rock-salt structure at 12.4 GPa. Derollez *et al* [18] measured acoustic and low frequency optical modes of $AgGaSe_2$ by inelastic neutron scattering and found large negative Grüneisen parameters for these modes. Roa *et al* [11] have reported pressure Raman measurements for $CuAlSe_2$ up to 30 GPa and observed a structural phase transition around 12 GPa.

Elastic constants of most of the chalcopyrite family of semiconductors have not been determined experimentally because of various difficulties in growing single crystals of these compounds [7]. Attempts have been made to fill this gap in the knowledge of the elastic properties of the chalcopyrites by theoretical calculations using different approaches, but mostly the results obtained differ considerably, and in many cases no satisfactory agreement has been achieved with existing experimental data. On the other hand, the availability of reliable elastic constant data is an essential prerequisite for any calculation or analysis of the influence of pressure, stress and strain on the properties of crystals and thin epitaxial layers.

In this paper, we present extensive first principles studies of the elastic, structural and lattice dynamical properties of chalcopyrite $CuAlSe_2$ under hydrostatic pressure. In section 2 we briefly review the underlying method and the parameters of the calculations. In the following section, the results are compared to experiments and tetrahedral binary compounds. Section 4 concludes the paper with a brief review of the main results.

2. Computational details

The present results have been obtained using the ABINIT code [19], that is based on pseudopotentials and plane waves. It relies on an efficient fast Fourier transform algorithm [20] for the conversion of wavefunctions between real and reciprocal space, on the adaptation to a fixed potential of the band-by-band conjugate gradient method [21] and on a potential-based conjugate-gradient algorithm for the determination of the self-consistent potential [22]. The exchange–correlation energy is evaluated in the local density approximation (LDA), using Perdew–Wang parametrization [23] of Ceperley–Alder electron–gas data [24].

The pseudopotentials have been generated with the FHI98PP code [25]. The details of choice of pseudopotentials were reported before for calculations of $CuInSe_2$ [26], $CuGaS_2$ [27] and $CuInS_2$ [28]. The kinetic energy cut-off needed to obtain a convergence better than 0.01 eV for total energy is found to be equal to 45 Ha. Changing the cut-off from 40 to 45 Ha changes response quantities by less than 1%. The Brillouin zone is sampled by 12 special k points, which is found to be enough for convergence of static as well as response calculations.

The ground state properties in the pressure free case are obtained by minimization of total energy with respect to the unit cell volume V. This is done by calculating the total energy for a number of fixed tetragonal distortion η values. For each η, the deformation parameter u is determined by minimizing the force on the atoms (η and u are more clearly defined in section 3.1). The equilibrium volume, bulk modulus and its pressure derivatives are calculated by fitting to a third-order Vinet equation of state [29]. The hydrostatic pressure is simulated by a uniform decrease in lattice constants a and c. For each compressed volume, the equilibrium value of u is recalculated from the force considerations.

Elastic and lattice dynamical properties are calculated within the framework of density functional perturbation theory. Technical details of the computation of responses to strain perturbations, atomic displacements and homogeneous electric fields can be found in [30]

Table 1. Calculated structural parameters of $CuAlSe_2$ compared to experimental data (a in au; η and u are dimensionless).

	This work	Ref. [33]	Ref. [34]	Ref. [17]	Ref. [35]
a	10.400	10.590	10.595	10.604	10.605
η	1.985	1.954	1.956	1.957	1.943
u	0.257	0.269	0.261	—	—

and [31], while [32] presents the subsequent computation of dynamical matrices, Born effective charges, dielectric permittivity tensors and interatomic force constants. The details of the calculation of elastic constants in linear response framework is given in [31].

3. Results

3.1. Atomic structure and lattice properties

The body-centred tetragonal chalcopyrite structure (space group D_{2d}^{12}, no. 122) can be derived from the cubic zinc-blende structure (space group T_d^2) by populating one of the face centred cubic sublattices with group VI atoms and other one with equal amounts of group I and III atoms in a regular fashion. Since, generally, I–VI and III–VI bond lengths, denoted by $d_{\mathrm{I-VI}}$ and $d_{\mathrm{III-VI}}$, respectively, are not equal, the mentioned substitution results in two different structural deformations: the first one is the relocation of anions in the x–y plane, which is characterized by the parameter $u = 0.25 + (d_{\mathrm{I-VI}}^2 - d_{\mathrm{III-VI}}^2)/a^2$. Here, a is the lattice constant in the x or y direction. The second consequence of differing anion–cation bond lengths is a deformation of the unit cell to a length c which is generally different from $2a$. This tetragonal distortion is characterized by the quantity $\eta = c/a$.

The zero-pressure lattice structural properties are obtained by energy and force minimization and compared to available experimental values in table 1. Considering the fact that the zero-point motion and thermal effects are not taken into account, the calculated a, η and u values agree with the experimental values quite well. The bulk modulus and its pressure derivative calculated by fitting to a third-order Vinet equation of state [29] are found to be 79.12 GPa and 4.55, which are in good agreement with available experimental bulk modulus values (85 $\pm$ 2 [17] and 85 $\pm$ 8 GPa [35]) as well as model calculations (71.16 [36] and 89.78 [37]) of $CuAlSe_2$.

Under pressure tetrahedrally coordinated chalcopyrite compounds undergo transformation to a denser phase with octahedral coordination [38], probably rock-salt structure. The phase transition pressure for $CuAlSe_2$ is around 12 GPa [17]. This pressure corresponds to a volume reduction of 15% if we use our calculated B_0 and B_0' values in the Vinet equation of state. Our calculations are done for the volume compression range (up to 10%) which is away from the phase transition point.

3.2. Elastic constants

There are a number of ways to calculate the elastic coefficients of a material from first principles. Until recently, the most widely used method was to deform the crystal from its equilibrium shape by a set of tetragonal and sheer deformations of various sizes and compute the resulting stress by using the quantum mechanical definition of stress [39]. Relationships between the applied strain and the calculated stress components provide a set of over-determined linear systems, which are solved by singular value decomposition to obtain the

Table 2. Independent elastic stiffness tensor components of $CuAlSe_2$ in units of GPa.

		C_{11}	C_{12}	C_{13}	C_{33}	C_{44}	C_{66}
$CuAlSe_2$	This work	102.9	63.4	65.7	104.5	42.8	41.5
$CuInSe_2$	This work	96.8	60.9	63.2	97.0	39.1	37.9
$CuInSe_2$	Ref. [40] (Exp.)	97.0	59.7	86.0	108.9	36.2	31.6
$CuInSe_2$	Ref. [41] (Theor.)	71.0	45.3	45.3	63.3	45.5	47.4

sought elastic stiffness constants. Recently, Hamann *et al* [31] developed a reduced coordinate metric tensor method for linear response formulation of strain type perturbations which could be calculated in density functional perturbation theory (DFPT). The elastic constants reported in this paper are obtained by the method of [31] as implemented in Abinit.

The elastic stiffness tensor of chalcopyrite compounds has six independent components because of the symmetry properties of the D_{2d}^{12} space group, namely $C_{11}, C_{33}, C_{44}, C_{66}, C_{12}$ and C_{13} in Young notation. The elastic compliance tensor elements of $CuAlSe_2$, which are calculated by using the method of metric tensor formulation of Hamann *et al* [31], are displayed in table 2. Elastic stiffness tensor components must satisfy certain relations known as Born stability criteria [42], which for the tetragonal chalcopyrite lattice requires that $C_{11}, C_{33}, C_{44}, C_{66} > 0$, $C_{11} > |C_{12}|$, $C_{11}C_{33} > C_{13}^2$, $(C_{11} + C_{12})C_{33} > 2C_{13}^2$. The values reported in table 2 satisfy all of these constraints. Since the experimental values are not available for $CuAlSe_2$, to give an idea about the expected experimental–theoretical spread, we display experimental, theoretical and calculated values for $CuInSe_2$ in the same table. Except for C_{13} ($\approx$25% underestimated) and C_{66} ($\approx$20% overestimated), the agreement between the calculated and experimental values is very good. The results obtained in this work seems to be much closer to the experimental values compared to those reported in [41]. The main ingredients of calculations in this work and [41] are similar, namely pseudopotential LDA-DFT. Although the methods of elastic constant calculations are different, results should converge to a common value. The pronounced difference in the results of these two sets of calculations might be due to lack of enough convergence in the calculations reported in [41]. Elastic constants reported in table 2 show that $CuAlSe_2$, also, displays pseudocubic elastic behaviour: for cubic crystals $C_{11}/C_{33} = C_{44}/C_{66} = C_{12}/C_{13} = 1$; from table 2 we find $C_{11}/C_{33} = 0.99, C_{44}/C_{66} = 1.03$ and $C_{12}/C_{13} = 0.97$ for $CuAlSe_2$. A similar behaviour, which is an expected result because of the u and η deformations being so small, was found for other Cu based chalcopyrites in [41].

One can define linear compressibilities for the pressure response of lattice constants for the a (κ_a) and c (κ_c) axes of the chalcopyrite structure [7]. κ_a and κ_c can be expressed in terms of elastic stiffness constants as

$$\kappa_a = -\frac{1}{a}\frac{\partial a}{\partial p} = \frac{C_{33} - C_{13}}{C_{33}(C_{11} + C_{12}) - 2C_{13}^2}$$

$$\kappa_c = -\frac{1}{c}\frac{\partial c}{\partial p} = \frac{C_{11} + C_{12} - 2C_{13}}{C_{33}(C_{11} + C_{12}) - 2C_{13}^2}.$$

Our calculated κ_a and κ_c are close, with values 4.4 and 4.0 TPa^{-1}, respectively. This finding partly justifies treating the effect of hydrostatic pressure on the lattice as uniform contraction of both a and c axes. Volume compressibility, which is defined as $\kappa = 2\kappa_a + \kappa_c$, is equal to 12.8 TPa^{-1}, which is similar to that reported for other chalcopyrite compounds [7].

The volume dependence of elastic constants is displayed in figure 1. As can be seen from the figure, C_{44} and C_{66} decrease linearly (nonlinearly) at low (high) pressure values while the other components increase with the compression of the lattice. Although the pressure

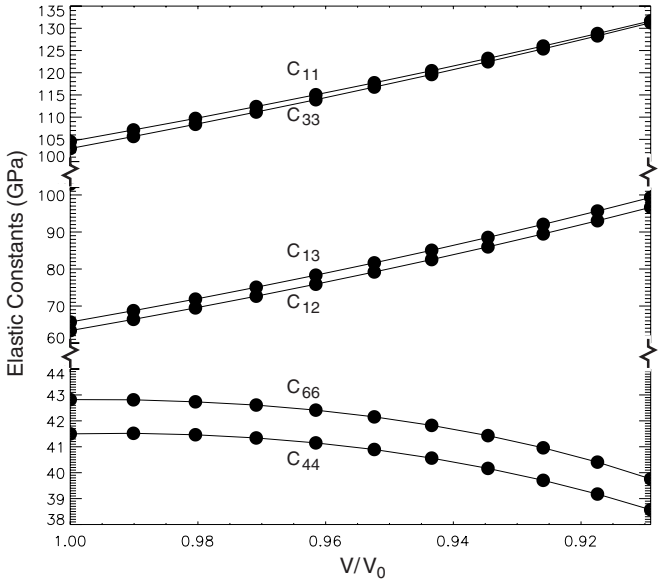

Figure 1. Volume dependence of the components of elastic stiffness components of $CuAlSe_2$.

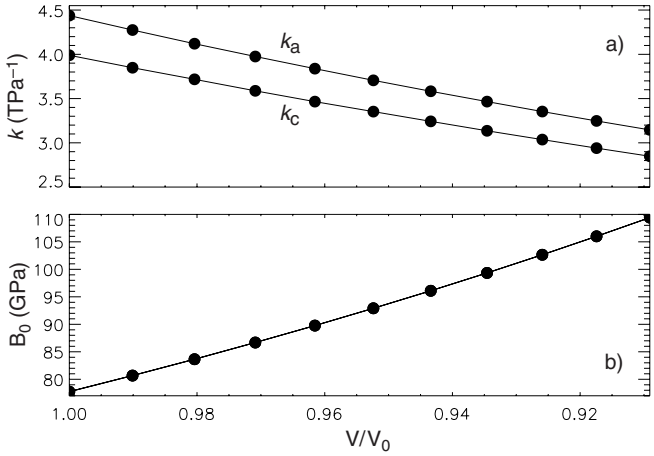

Figure 2. Volume dependence of (a) linear compressibilities (κ_a and κ_c) and (b) the bulk modulus of $CuAlSe_2$.

dependence of elastic constants of $CuAlSe_2$ is not available experimentally, elastic constants of a similar compound $CdGaAs_2$ show similar properties at low pressures [7]. Volume dependences of κ_a and κ_c are displayed in figure 2 along with the volume dependence of the bulk modulus. Both compressibilities (bulk modulus) decrease (increase) uniformly with increasing pressure.

3.3. Born effective charges

For insulators, the Born effective charge is a measure of the change in electronic polarization due to ionic displacements. For atom κ, $Z^{\star}_{\kappa,\beta\alpha}$, quantifies, to linear order, the polarization per

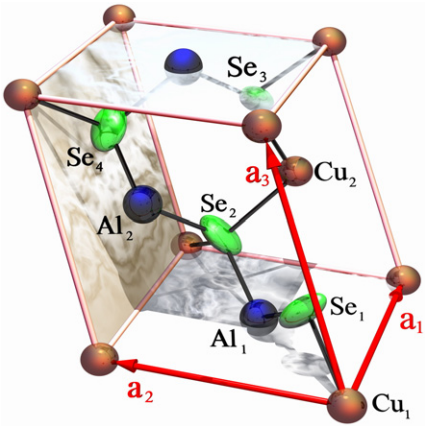

Figure 3. Dynamical Born effective charges of chalcopyrite $CuAlSe_2$. Here, for each atom the unit sphere is transformed by the effective charge tensor of that atom. Al and Se spheres are further scaled by 1/3 and 1/2, respectively, for visual clarity.

(This figure is in colour only in the electronic version)

unit cell, created along the direction β when the atoms of sublattice κ are displaced along the direction α, under the condition of zero electric field. Computationally, it is the mixed second derivative of the total energy with respect to the macroscopic field component E_α and the β component of the displacement of the κth particle.

In table 3, we display dynamical effective charge tensors, eigenvalues of symmetric parts of these tensors and Grüneisen parameters of these eigenvalues, $\gamma^\star$, which is defined as

$$\gamma^\star = -\frac{\mathrm{d}\ln\lambda}{\mathrm{d}\ln V}$$

where V is the unit cell volume and λ is the eigenvalue of the symmetric part of the relevant effective charge tensor. The effective charge tensors are also displayed graphically in figure 3. Because of finite k-point sampling there is a deviation from charge neutrality which is less than 0.01 electron for the unit cell. The first thing to consider from table 3 is that if Cu, Al and Se in $CuAlSe_2$ are considered as $+1$, $+3$ and -2 ions, the dynamical charges show no anomalous behaviour, which is expected because such anomalous effective dynamical charges are observed for ferroelectrically unstable semiconductors as well as near metallic and strongly correlated electronic systems [43], and $CuAlSe_2$ has none of these properties.

The form of effective charge tensor for the constituents is determined by the site symmetry of the ions. $Z^\star$ of cations, which have same site symmetry (they are located at 4*a* and 4*b* Wyckoff positions) are almost diagonal with an anisotropy of $\approx$9% for Cu and $\approx -5\%$ for Al. These anisotropies are higher than those seen in $CuAlS_2$ [44], but still low enough that the shapes of Cu and Al in figure 3 are almost spherical. The shape of $Z^\star$ for the Se ion is markedly different from that of cations as can be seen from table 3 and figure 3. Se ions are located at lower symmetry sites (8*d* positions) and as a result their effective charge tensors have nonequivalent diagonal components as well as sizable off-diagonal components. The tetrahedral shifting of anion atoms creates four different configurations for these atoms and the resulting effective charge tensor elements can be divided into two classes according to the direction of the tetrahedral shifting being along the x or y direction. $Z^\star_{\mathrm{Se},zz} = -1.64$ for all anions while $Z^\star_{\mathrm{Se},xx}$ and $Z^\star_{\mathrm{Se},yy}$ take the value -1.50 or -1.71 depending on the direction of u. Also, depending on the u distortion being along the x or y direction, the off-diagonal

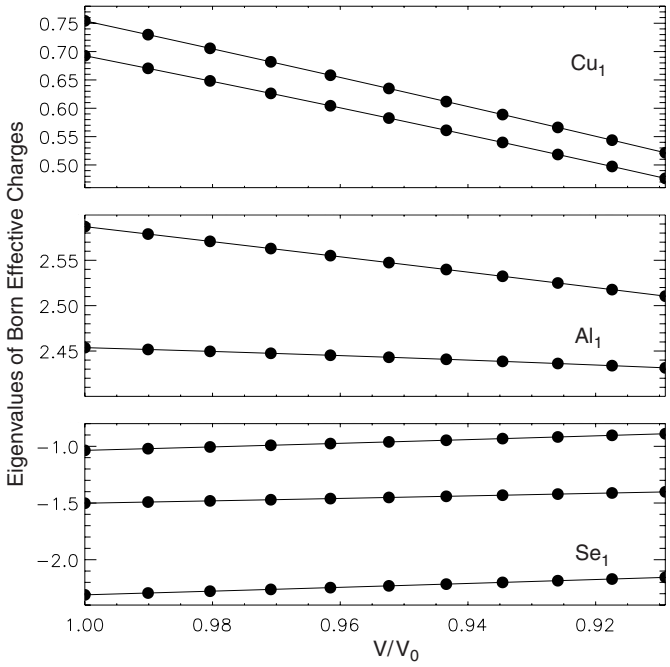

Figure 4. Volume dependent Born effective charges of $CuAlSe_2$.

Table 3. Calculated Born effective charges of $CuAlSe_2$. The eigenvalues, λ, of the symmetric part of $Z^\star$ are given in brackets. The last column is the Grüneisen parameter, $\gamma^\star$, for the effective charge.

		λ	$\gamma^\star$
$Z^\star_{Cu}$	$\begin{pmatrix} 0.75 & 0.09 & 0.00 \\ -0.09 & 0.75 & 0.00 \\ 0.00 & 0.00 & 0.69 \end{pmatrix}$	$\begin{bmatrix} 0.75 \\ 0.75 \\ 0.69 \end{bmatrix}$	$\begin{bmatrix} -3.25 \\ -3.25 \\ -3.23 \end{bmatrix}$
$Z^\star_{Al}$	$\begin{pmatrix} 2.45 & 0.02 & 0.00 \\ -0.02 & 2.45 & 0.00 \\ 0.00 & 0.00 & 2.59 \end{pmatrix}$	$\begin{bmatrix} 2.45 \\ 2.45 \\ 2.59 \end{bmatrix}$	$\begin{bmatrix} -0.08 \\ -0.08 \\ -0.32 \end{bmatrix}$
$Z^\star_{Se_1}$	$\begin{pmatrix} -1.50 & 0.00 & 0.00 \\ 0.00 & -1.71 & 0.62 \\ 0.00 & 0.65 & -1.64 \end{pmatrix}$	$\begin{bmatrix} -2.31 \\ -1.50 \\ -1.04 \end{bmatrix}$	$\begin{bmatrix} -0.71 \\ -0.69 \\ -1.47 \end{bmatrix}$
$Z^\star_{Se_3}$	$\begin{pmatrix} -1.71 & 0.00 & 0.62 \\ 0.00 & -1.50 & 0.00 \\ 0.65 & 0.00 & -1.64 \end{pmatrix}$	$\begin{bmatrix} -2.31 \\ -1.50 \\ -1.04 \end{bmatrix}$	$\begin{bmatrix} -0.71 \\ -0.69 \\ -1.47 \end{bmatrix}$

components $Z^\star_{Se,zx}$, $Z^\star_{Se,xz}$ or $Z^\star_{Se,yz}$, $Z^\star_{Se,zy}$ are different than zero. Hence, the shape of the effective charge tensor for the anions is far from being spherical, which has also been observed for other members of the Cu-based chalcopyrite family of semiconductors.

As can be seen from table 3, the Grüneisen parameters for the dynamical effective charges of all the ions are negative, which indicate that $Z^\star$ decreases with increasing pressure. The eigenvalues of the symmetric part of the effective charge tensors are displayed as a function of the volume in figure 4. The most important conclusion from the effective charge Grüneisen parameters in table 3 and the graphs in figure 4 is that the Born effective charges decrease linearly with pressure in the considered pressure range. Pressure induced reduction of effective

Table 4. Static and high frequency dielectric tensor components of $CuAlSe_2$.

	$\epsilon_\infty^\parallel$	$\epsilon_\infty^\perp$	ϵ_∞	$\epsilon_0^\parallel$	$\epsilon_0^\perp$	ϵ_0
This work	8.07	8.22	8.17	9.99	9.74	9.82
Ref. [14]	5.2	6.0	5.7	6.67	8.28	7.74
Ref. [46]	6.0	6.2	6.1	8.4	8.6	8.5

charges indicates that a charge redistribution in comparison with the zero-pressure situation is found to be the case for almost all zinc-blende materials, except SiC [45].

3.4. Dielectric permittivity tensors

The form of the dielectric tensor is determined by the symmetry of the crystal. Our calculated electronic (ϵ_∞) and static (ϵ_0) dielectric tensors have two independent components $\epsilon^\parallel$ and $\epsilon^\perp$ along and perpendicular to the c axis, respectively. While the electronic dielectric tensor is almost isotropic, ϵ_0 has a small ($\approx$2.5%) anisotropy, which is consistent with the fact that for $CuAlSe_2$ tetragonal distortion is very small ($\eta = c/a \approx 2$).

We display our calculated dielectric tensor components along with model calculations of [46] and experimentally available values in table 4. The averages of ϵ_∞ and ϵ_0, obtained from the expression ϵ_∞ (or ϵ_0) $= (2\epsilon_\infty^\perp + \epsilon_\infty^\parallel)/3$, are also shown in this table.

The infrared data for the electronic part of the dielectric tensor elements of $CuAlSe_2$ are similar and around 5.7. It is well known that the density functional theory (DFT) overestimates the high-frequency dielectric constants; this is a well known problem related to underestimation of the bandgap in DFT [47–49]. Our calculated ϵ_∞ values are somewhat higher than the expected overestimation. For the high frequency components the experimental $\epsilon_\infty^\perp > \epsilon_\infty^\parallel$ relation is found to hold for the calculated results but the same relation for the static components is found to change direction, in contradiction to experimental results.

One can define a Grüneisen parameter

$$\gamma^\epsilon = -\frac{\mathrm{d}\ln\epsilon}{\mathrm{d}\ln V}$$

for the pressure dependence of the dielectric constants. We have found that the Grüneisen parameters of the electronic part of both perpendicular and parallel components of dielectric tensor are negative with similar magnitudes ($\gamma^{\epsilon_\infty^\perp} = -0.126$ and $\gamma^{\epsilon_\infty^\parallel} = -0.132$), which are somewhat lower than the values found for zinc-blende compounds [45]. The static constants show a similar trend, with markedly higher Grüneisen parameters ($\gamma^{\epsilon_0^\perp} = -0.64$ and $\gamma^{\epsilon_0^\parallel} = -0.52$). It should be noted that the relative difference between $\gamma^{\epsilon_0^\perp}$ and $\gamma^{\epsilon_0^\parallel}$ (0.19) is higher than that for $\gamma^{\epsilon_\infty^\perp}$ and $\gamma^{\epsilon_\infty^\parallel}$ (-0.05).

Figure 5 displays our calculated volume-dependent static and high frequency dielectric tensor components. All of the components decrease under pressure; the volume dependence of static (high frequency) components is slightly (highly) nonlinear, especially at higher pressures, which is similar to what has been found for the most tetrahedrally coordinated semiconductors.

3.5. Zone centre phonons

Since the body-centred tetragonal unit cell of the chalcopyrite structure has eight atoms, there are a total of 24 modes of vibration. A detailed discussion of group theoretical properties of chalcopyrite zone centre phonons can be found in [27] and [50]. The irreducible representation

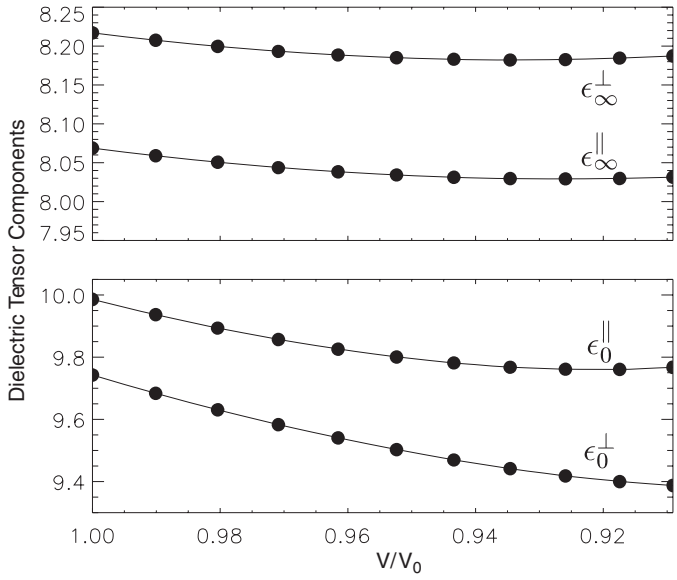

Figure 5. Volume dependent static and high frequency dielectric tensor components of $CuAlSe_2$.

at the centre of the Brillouin zone is

$$\Gamma_{\text{opt}} = 1\Gamma_1 \oplus 2\Gamma_2 \oplus 3\Gamma_3 \oplus 3\Gamma_4 \oplus 6\Gamma_5$$

for optical modes, and

$$\Gamma_{\text{aco}} = 1\Gamma_4 \oplus 1\Gamma_5$$

for acoustic modes.

In table 5 our calculated zone centre phonon frequencies, their symmetry assignments and mode Grüneisen parameters are displayed and compared with infrared [12–14] and Raman [8–12] spectroscopic measurements. The most striking thing about the experimentally available data in table 5 is that except Γ_1 and the highest frequency Γ_4 and Γ_5 modes, there are very large differences among all phonon mode frequencies. The zone centre phonon frequencies of Cu-based chalcopyrite semiconductors, generally, are clearly grouped into three branches: low, medium and high frequency. IR data reported by [14] is at odds with this trend and its low frequency Γ_4 and intermediate frequency Γ_5 modes are either overtones or come from a modification of the chalcopyrite structure. Our calculated results agree best with the Raman and IR measurements reported by [12] with an average relative root-mean square deviation of around 9%, which is within the range of expected accuracy of DFT response calculations.

The Grüneisen parameter γ_i for phonon mode i is defined as

$$\gamma_i = -\frac{\mathrm{d}\ln\omega_i}{\mathrm{d}\ln V}$$

where ω_i is the frequency of mode i and V is the unit cell volume of the crystal. γ_i expresses the change in phonon frequency under hydrostatic pressure. In table 5 we also display and compare our calculated mode Grüneisen parameters with experimental values reported in [11]. One of the interesting properties of phonons of tetrahedrally coordinated semiconductors of diamond and zinc-blende structure is the pressure softening of their transverse acoustic (TA) modes. Mode Grüneisen parameters for TA modes of group IV, III–V and II–VI compounds that

Table 5. Frequencies of phonons and mode Grüneisen parameters at the Γ point (ω in cm^{-1}).

	Ab initio	Experiment								γ_i	
Mode	Present	IR [13]	IR [14]	IR [12]	R [8]	R [9]	R [10]	R [11]	R [12]	Present	Ref. [11]
Γ_1	192				186	189	185	185	187	1.5	1.4
Γ_2	218									1.2	
Γ_2	181									1.6	
Γ_3	381					233	207	311	∼315	1.2	1.5
Γ_3	191				213		124	214	214	1.9	1.1
Γ_3	96						87	60	124	0.02	1.5
Γ^{LO}_{4TO}	389	375	401	382		373			384	1.3	
	358	350	370	340	358		389		342	1.5	
Γ^{LO}_{4TO}	204		349	193				264		2.2	
	200		342	186			360			2.3	0.5
Γ^{LO}_{4TO}	90		260	84	85	89		93	89	−0.5	−0.1
	89		252	84	60		60	88		−0.6	0.1
Γ^{LO}_{5TO}	398	395	396	398		388		395	398	1.1	0.8
	373	360	393	366	395		394		366	1.2	
Γ^{LO}_{5TO}	361	350	382	350		266		367	351	1.5	1.0
	359	340	354	346			364		347	1.6	
Γ^{LO}_{5TO}	200		348	186		197		344		2.5	1.1
	198		343	184	342		343			2.5	
Γ^{LO}_{5TO}	171		237	164		165		245		2.2	0.6
	170		229	161	161		162		161	2.3	
Γ^{LO}_{5TO}	106		159	111		112		160		−0.8	0.6
	106		156	110			112	159	113	−0.8	2.4
Γ^{LO}_{5TO}	65		80			67		81	61	−1.9	0.04
	65		79				106	78		−1.9	0.1
		Rms relative deviations									
		0.035	0.332	0.053	0.232	0.232	0.371	0.265	0.094		

crystallize in diamond and zinc-blende structure are all negative towards the Brillouin zone boundaries [51]. As the chalcopyrite structure is obtained by doubling and deforming the zinc-blende structure, the first Brillouin zone (BZ) of chalcopyrite is formed by folding the zinc-blende BZ. The correspondence between the chalcopyrite zone centre phonon modes and modes in zinc-blende structure has been given in [50, 52–54]. We have found three negative mode Grüneisen parameters for $CuAlSe_2$, which are two low frequency optical Γ_5 and one low frequency Γ_4 modes. These modes originate from X_{5ac}, W_{4ac} and W_{2ac} modes of zinc-blende structure, respectively. γ for the X_{5ac}-originated mode is similar in magnitude and sign to values reported for zinc-blende structures [55–58]. Frequency and mode Grüneisen parameters at the W point for zinc-blende materials are, unfortunately, not as well known as those at the X point. From the available data [55] we would expect a smaller, but still negative, Grüneisen parameter. Experimental γ values for these two modes seem to be very small but positive.

For zinc-blende materials, the mode Grüneisen parameter for longitudinal optical phonon modes (γ_{TO}) is generally higher than that of the transverse optical mode (γ_{LO}) [55], which is interpreted as a reflection of a decrease in ionicity with increasing pressure. We have found a similar relationship for $CuAlSe_2$ for the polar modes (the highest frequency Γ_5 and Γ_4 modes) originating from the zone-centre polar mode (Γ_{15}) of the zinc-blende structure.

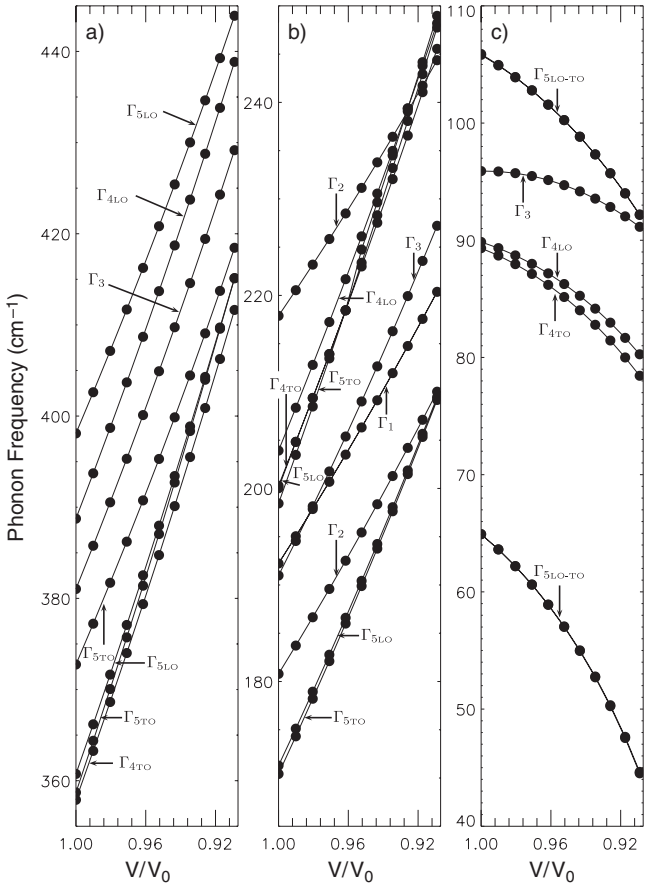

Figure 6. Volume dependence of phonon frequencies for $CuAlSe_2$ at the Γ point.

The volume dependent zone centre phonon frequencies of $CuAlSe_2$ are shown in figure 6. High and intermediate frequency modes, which are displayed in figures 6(a) and (b) respectively, show a similar volume dependence; their frequencies increase linearly with pressure at different rates. The volume dependence of the low frequency branch, which is displayed in figure 6(c), is completely different compared to the intermediate and high frequency branches. Two Γ_{5LO-TO} and Γ_{4LO-TO} modes decrease with volume reduction as expected from their negative mode Grüneisen parameter; in addition the Γ_3 mode frequency starts decreasing after a volume reduction to 97%. Furthermore, the volume dependence of these modes is far from linear, especially for the Γ_4 mode.

4. Conclusion

We have investigated the pressure dependent lattice dynamical properties, such as Born effective charge tensor, Brillouin zone centre phonon frequencies, and static and high frequency dielectric tensors and elastic compliance tensors of ternary semiconductor $CuAlSe_2$ within the density functional perturbation theory framework. We have found that the pressure dependences of these quantities show similar trends with binary tetrahedrally coordinated

compounds. Under hydrostatic pressure, the dynamical effective charges decrease. The zone centre modes originating from the modes with negative Grüneisen parameter in zinc-blende materials have negative Grüneisen parameters and the ordering of $\gamma_{TO} > \gamma_{LO}$ is respected for the zone-centre chalcopyrite modes that originate from the zone-centre polar mode of the zinc-blende structure.

Acknowledgments

This work was supported by Tübitak under grant no. TBAG-2449(104T059) and AIBU Research Fund grant no. 04.03.02.199.

References

[1] Gaber A M, Tuttle J R, Albin D S, Tennant A L and Contreras M A 1994 *12th NREL Photovoltaic Program Review* (*AIP Conf. Proc.* vol 306) ed R Noufi (New York: AIP) p 59
[2] Birkmire R W and Eser E 1997 *Annu. Rev. Mater. Sci.* **27** 625
[3] Shirakata S, Chichibu S, Matsumoto S and Isomura S 1993 *Japan. J. Appl. Phys.* **32** L167
[4] Chichibu S, Shirakata S, Isomura S, Harada Y, Uchida M, Matsumoto S and Higuchi H 1995 *J. Appl. Phys.* **77** 1225
[5] Bodnar I V, Rud V Y and Rud Y V 1994 *Tech. Phys. Lett.* **20** 317
[6] Ohrendorf F W and Haeuseler H 1999 *Cryst. Res. Technol.* **34** 339
[7] Neumann H 2004 *Cryst. Res. Technol.* **39** 939
[8] Gebicki W, Filipowicz J and Bacewicz R 1996 *J. Phys.: Condens. Matter* **8** 8695
[9] Azuhata T, Terasako T, Yoshida K, Sota T, Suzuki K and Chichibu S 1996 *Physica* B **219** 496
[10] Azhnuk Y N, Artamonov V V and Bodnar I V 1985 *J. Appl. Spectrosc.* **43** 1276
[11] Roa L, Chervin J C, Chevy A, Davila M, Grima P and González J 1996 *Phys. Status Solidi* b **198** 99
[12] Eifler A, Kudritskaya E A, Bodnar I V and Riede V 2003 *J. Phys. Chem. Solids* **64** 1983
[13] Bodnar I V, Karoza A G, Smirnova G I and Smirnova T V 1990 *Zh. Prikl. Spektrosk.* **53** 677
[14] Andriesh A M, Syrbu N N, Iovu M S and Tezlavan V E 1995 *Phys. Status Solidi* b **187** 83
[15] Anastassakis E and Cardona M 1998 *High Pressure Semiconductor Physics* vol 55, ed T Suski and W Paul (New York: Academic)
[16] Gonzalez J, Fernandez B J, Besson J M, Gauthier M and Polian A 1992 *Phys. Rev.* B **46** 15092
[17] Roa L, Chervin J C, Itié J P, Polian A, Gauthier M and Chevy A 1999 *Phys. Status Solidi* b **211** 455
[18] Derollez P, Klotz S, Lazewski J, Braden M, Hennion B, Fouret R and Gonzalez J 2002 *High Pressure Res.* **22** 283
[19] Gonze X, Beuken J-M, Caracas R, Detraux F, Fuchs M, Rignanese G-M, Sindic L, Verstraete M, Zerah G, Jollet F, Torrent M, Roy A, Mikami M, Ghosez Ph, Raty J-Y and Allan D C 2002 *Comput. Mater. Sci.* **25** 478 http://www.abinit.org
[20] Goedecker S 1997 *SIAM J. Sci. Comput.* **18** 1605
[21] Payne M C, Teter M P, Allan D C, Arias T A and Joannopoulos J D 1992 *Rev. Mod. Phys.* **64** 1045
[22] Gonze X 1996 *Phys. Rev.* B **54** 4383
[23] Perdew J P and Wang Y 1992 *Phys. Rev.* B **45** 13244
[24] Ceperley D M and Alder B J 1980 *Phys. Rev. Lett.* **45** 566
[25] Fuchs M and Scheffler M 1999 *Comput. Phys. Commun.* **119** 67
[26] Parlak C and Eryiğit R 2002 *Phys. Rev.* B **66** 165201
[27] Akdoğan M and Eryiğit R 2002 *J. Phys.: Condens. Matter* **14** 7493
[28] Eryiğit R, Parlak C and Eryiğit R 2003 *Eur. Phys. J.* B **33** 251
[29] Vinet P, Rose J H, Ferrante J and Smith J R 1989 *J. Phys.: Condens. Matter* **1** 1941
[30] Gonze X 1997 *Phys. Rev.* B **55** 10337
[31] Hamann D R, Wu X, Rabe K M and Vanderbilt D 2005 *Phys. Rev.* B **71** 035117
[32] Gonze X and Lee C 1997 *Phys. Rev.* B **55** 10355
[33] Spiess H W, Heaberlen U, Brandt G, Räuber A and Schneider J 1974 *Phys. Status Solidi* b **62** 183
[34] Bodnar I V 2002 *Inorg. Mater.* **38** 647
[35] Kumar R S, Sekar A, Jaya N V, Natarajan S and Chichibu S 2000 *J. Alloys Compounds* **312** 4
[36] Meng Q B, Xiao C Y, Wu Z J, Feng K-A, Lin Z D and Zhang S Y 1998 *Solid State Commun.* **107** 369

[37] Reddy R R, Ahammed Y N, Gopal K R, Azeem P A, Rao T V R and Reddy P M 2000 *Opt. Mater.* **14** 355
[38] Werner A, Hochheimer H D and Jayaraman A 1981 *Phys. Rev.* B **23** 3836
[39] Nielsen O H and Martin R M 1983 *Phys. Rev. Lett.* **50** 697
[40] Fouret R, Hennion B, Gonzalez J and Wasim S M 1993 *Phys. Rev.* B **47** 8269
[41] Lazewski J, Neumann H, Jochym P T and Parlinski K 2003 *J. Appl. Phys.* **93** 3789
[42] Born M and Huang K 1954 *Dynamical Theory of Crystal Lattices* (Oxford: Clarendon)
[43] Filippetti A and Spaldin N A 2003 *Phys. Rev.* B **68** 045111
[44] Parlak C and Eryiğit R 2004 *Phys. Rev.* B **70** 075210
[45] Debernardi A, Ulrich C, Cardona M and Syassen K 2001 *Phys. Status Solidi* b **223** 213
[46] Márquez R and Rincón C 1995 *Phys. Status Solidi* b **191** 115
[47] Gonze X, Ghosez Ph and Godby R W 1995 *Phys. Rev. Lett.* **74** 4035
[48] Martin R M and Ortiz G 1997 *Phys. Rev.* B **56** 1124
[49] Ghosez Ph, Gonze X and Godby R W 1997 *Phys. Rev.* B **56** 12811
[50] Tanino H, Maeda T, Fujikake H, Nakanishi H, Endo S and Irie T 1992 *Phys. Rev.* B **45** 13323
[51] Trommer R, Anastassakis E and Cardona M 1976 *Light Scattering in Solids* ed M Balkanski, R C C Leite and S P S Porto (New York: Wiley) p 396
[52] Talwar D N and Agrawal B K 1974 *Phys. Status Solidi* b **64** 71
[53] Holah G D, Webb J S and Montgomery H 1974 *J. Phys. C: Solid State Phys.* **7** 3875
[54] Mintairov A M, Sadchikov N A, Sauncy T, Holtz M, Seryogin G A, Nikishin S A and Temkin H 1999 *Phys. Rev.* B **59** 15197
[55] Trommer R, Müller H, Cardona M and Vogl P 1980 *Phys. Rev.* B **21** 4869
[56] Debernardi A and Cardona M 1996 *Phys. Rev.* B **54** 11305
[57] Iakovenko E V, Gauthier M and Polian A 2003 *Preprint* cond-mat/0301045
[58] Kunc K and Martin R M 1981 *Phys. Rev.* B **24** 2311